JOINT EUROPEAN TORUS JET

JET–P(87)29

T. Hellsten and L. Villard

Power Deposition for Ion Cyclotron Heating in Large Tokamaks

Power Deposition for Ion Cyclotron Heating in Large Tokamaks

T. Hellsten and L. Villard[1]

JET-Joint Undertaking, Culham Science Centre, OX14 3DB, Abingdon, UK

[1]*Centre de recherches en physique des plasmas, Association Euratom-Confédération Suisse, Ecole poly technique fédérale de Lausanne, Lausanne, Switzerland.*

Preprint of Paper to be submitted for publication in
Nuclear Fusion

POWER DEPOSITION FOR ION CYCLOTRON HEATING IN LARGE TOKAMAKS

T. Hellsten and L. Villard*

JET Joint Undertaking, Abingdon, OX14 3EA, United Kingdom.

*CRPP, Association Euratom - Confederation Suisse, École Polytechnique Fédérale de Lausanne, Lausanne, Switzerland.

Abstract

The power deposition profiles during minority ion-cyclotron heating are analysed in large tokamaks by using the global, toroidal wave code LION. For tokamaks with large aspect ratio and with circular cross-section, the wave is focused on the magnetic axis and can be absorbed there by cyclotron absorption when the cyclotron resonance passes through the magnetic axis. The power deposition profile is then essentially determined by the Doppler broadening of the ion-cyclotron resonance. For equilibria either non-circular or with a small aspect ratio the power deposition profile depends also on the strength of the damping. In this case the power deposition profile can be expressed as a sum of two power deposition profiles. One is related to the power absorbed in a single pass, and its shape is similar to that obtained for large aspect ratio and circular cross-section. The other profile is obtained by calculating the power deposition in the limit of weak damping, in which case the wave electric field is almost constant along the cyclotron resonance layer. An heuristic formula for the power deposition is given. The formula includes a number of calibration curves and functions which has been calculated with the LION code for JET relevant equilibria. The formula enables one to calculate the power

deposition in a simple way when the launched wave spectrum and damping coefficients are known.

1. Introduction

Ion cyclotron heating by the fast magnetosonic wave has recently become an often used supplementary heating method in tokamaks. The absorption of the wave due to ion cyclotron heating occurs in the neighbourhood of the cyclotron resonances or their harmonics. Since these resonances may intersect the whole plasma volume it is important to determine where on these resonances the power is absorbed. To know the power density is important for determining the distortion of the velocity distribution of the heated ions which in turn will determine energy transfer to electrons and bulk ions, the modification of the absorption, and the enhancement of fusion reactivity in case the heated species undergoes fusion reactions. To calculate the power deposition one has to solve the wave equation for the magnetosonic wave, which is a rather complicated partial differential equation, in a non-trivial geometry. In tokamak geometry only the toroidal angle becomes an ignorable coordinate. The wave field has then to be calculated by numerical methods. Two numerical methods have been adopted for this problem; ray tracing techniques [1,2] and global wave calculations with finite element methods [3-5]. Each method has both advantages and disadvantages. With the global wave calculations one can, in principle, solve the wave equation with appropriate boundary conditions and include mode conversion in a self-consistent way. However, the method suffers in that it requires large computer space and long computing times to obtain sufficient accuracy, e.g. the calculation of the power deposition with the LION code [4] for a mesh having 5000 cells takes about 40 seconds on a CRAY1 and needs 130,000 words of central memory storage. The disadvantage of the ray tracing technique is

much more fundamental. It is not valid close to the plasma boundary and cannot treat cavity resonances.

In this paper we analyse what determines the power deposition profile in a tokamak plasma where the wave is launched from the low field side, using a global wave code. A simplified model for calculating the power deposition is given for the case where the power is absorbed along one cyclotron resonance. In Section 2 a formula for the power deposition is given for the case where the cyclotron resonance passes through the magnetic axis. In Section 3 a formula for off-axis heating is given for a particular shape of the plasma cross-section.

2. Analysis of the power deposition

To calculate wave field and power deposition during ion cyclotron heating we use the global wave code LION [4]. This code solves the wave equation which in the limit of zero electron mass and zero electron and ion gyro radius takes the following form in toroidal geometry

$$\left(\nabla\times\nabla\times\underline{E}_\perp = \frac{\omega^2}{c^2}\,\underline{\underline{\varepsilon}}\,\underline{E}_\perp\right)_\perp = 0 \tag{1}$$

where $\underline{\underline{\varepsilon}}$ is an operator given by

$$\underline{\underline{\varepsilon}} = \begin{pmatrix} \varepsilon_{NN} & \varepsilon_{N\Lambda} \\ -\varepsilon_{N\Lambda} & \varepsilon_{NN} \end{pmatrix} + \left(\frac{c}{\omega}\right)^2 \frac{\vec{B}_o\cdot\mathrm{rot}\,\vec{B}_o}{B_o^2} \begin{pmatrix} \mathrm{rot}_N\,\vec{e}_N & \mathrm{rot}_N\,\vec{e}_\Lambda \\ \mathrm{rot}_\Lambda\,\vec{e}_N & \mathrm{rot}_\Lambda\,\vec{e}_\Lambda \end{pmatrix}, \tag{2}$$

$$\varepsilon_{NN} = \varepsilon_\perp^o\left(k_z = \frac{n}{R}\right),\quad \varepsilon_{N\Lambda} = \varepsilon_{xy}^o\left(k_z = \frac{n}{R}\right),$$

$$\varepsilon_{\perp}^{o} = \sum_{\alpha} \frac{\omega_{p\alpha}^{2}}{2|k_z| v_{th\alpha} \omega} \left(Z_1^{(\alpha)} + Z_{-1}^{(\alpha)}\right), \quad \varepsilon_{xy}^{o} = i\Sigma_{\alpha} \frac{\omega_{p\alpha}^{2}}{2|k_z| v_{th\alpha} \omega} \left(Z_1^{(\alpha)} - Z_{-1}^{(\alpha)}\right)$$

$$Z_{\ell}^{(\alpha)} = Z\left(\frac{\omega - \ell\omega_{c\alpha}}{|k_z| v_{th\alpha}}\right)$$

in a coordinate system described by the unit vectors

$$\vec{e}_N = \nabla\psi / |\nabla\psi|, \quad \vec{e}_\Lambda = \vec{e}_{\shortparallel} \times \vec{e}_N, \quad \vec{e}_{\shortparallel} = \vec{B}_o / B_o.$$

$\varepsilon_{\perp}^{o}$, ε_{xy}^{o} denote the components of the dielectric tensor in the limit of zero gyro radius in a local cartesian coordinate system where the z-direction is parallel to the magnetic field. For the calculation of $\varepsilon_{\perp}^{o}$ and ε_{xy}^{o} we approximate k_z by n/R, where n is the toroidal mode number and R is the distance to the axis of the torus. Z denotes the Fried-Conte function. No phenomenological damping as mentioned in Ref. [4] is being used in this paper. The second term in the dielectric tensor appears due to the finite equilibrium current along the magnetic field [6].

For the power deposition we study the Poynting flux through a magnetic surface

$$\bar{P}(s) = \frac{c}{4\pi} \int (\underline{E} \times \underline{B}) \cdot d\underline{\Sigma} \, . \tag{3}$$

Instead of using the magnetic flux, ψ, to label the flux surfaces, we use a variable, s, such that $s \propto \sqrt{\psi}$. The variable s is zero on the magnetic axis and is normalised to 1 at the plasma boundary. The advantage of using s is that it is nearly proportional to the minor radius of the plasma.

The power density averaged over a magnetic surface, p, is obtained by

differentiating $\bar{P}(s)$ with respect to the enclosed volume, V,

$$p = \frac{d\bar{P}}{ds} \Big/ \frac{dV}{ds} \tag{4}$$

In Fig. 1 we give $(dV/ds)/R_o^3 s$ for an elliptic JET equilibrium, where R_o is the radius of the magnetic axis. For this equilibrium the radius of the magnetic axis, the aspect ratio, the ellipticity and the triangularity of the plasma boundary are 309cm, 2.6, 1.4 and 0.19 respectively.

In this section we restrict our study to the case where the ion cyclotron resonance passes through the magnetic axis and when ion cyclotron absorption is the only absorption mechanism.

When comparing the results of the LION code for different equilibria we have found that the power deposition profile for equilibria with circular cross-section and large aspect ratio differ in the functional form from that for other equilibria. For equilibria with large aspect ratio, circular cross-section and a low minority concentration, the plasma boundary acts as a mirror, focusing the wave field on the magnetic axis, as can be seen in Fig. 2a. For equilibria with a non-circular cross-section or with small aspect ratio, the regular field structure is destroyed as can be seen in Fig. 2b. In case of large minority concentrations when a cut-off appears on the high field side of the cyclotron resonance of the minority species, the wave field will also spread along the cyclotron resonance. This appears also for the small toroidal mode numbers when dispersion due to the "poloidal mode" numbers becomes important. The lack of focusing of the wave field for these cases leads to a large field along the entire cyclotron resonance and hence the power deposition becomes less peaked. Figure 3 shows the magnetic surface averaged Poynting flux $\bar{P}$ versus s for equilibria with an aspect ratio of 10 but with different ellipticities during minority heating of hydrogen in

deuterium with flat density profile and the following parameters: n_D = $3\times10^{13}cm^{-3}$, n_H = $7.5\times10^{10}cm^{-3}$, T_H = 10keV, f = 33MHz and n = 30, where n is the toroidal mode number. Similar results are obtained for circular cross-sections when the aspect ratio is varied. The large aspect ratio approximation is found to be valid for equilibria with aspect ratios larger than 5.

For an antenna located on the low field side and for equilibria having a large aspect ratio and circular cross-section we use the following ansatz to describe the flux surface averaged Poynting flux, $\bar{P}_1(s)$,

$$\bar{P}_1(s) = \bar{P}_1(1)\{1 - \exp[-(s/s_o)^2 \ln 2]\}/[1 - \exp[-(1/s_o)^2 \ln 2]] \qquad (5)$$

This ansatz is found to fairly well describe the power deposition when the wave is focussed on the magnetic axis and when the minor radius is large compared to a wavelength. The half width, s_o, is calculated with the code. In Fig. 4a we plot s_o against a parameter $d = n\sqrt{\langle v_\parallel^2\rangle}/\omega r_o$, which determines the Doppler broadening of the cyclotron resonance. $\langle v_\parallel^2\rangle$ = 2kT/m is the parallel velocity squared of the heated ions averaged over the velocity space, $\omega/2\pi$ is the wave frequency and r_o is the minor radius at the midplane on the outboard side. The calculations have been performed for various heating scenarios, densities, temperatures and toroidal mode numbers: hydrogen minority in deuterium with a concentration of 4% and helium-3 minority in deuterium with a concentration varied between 4% and 10%; central deuterium density n_{DO} = $4\cdot10^{19}$ to $1\cdot10^{20}m^{-3}$, two different density profiles; central minority temperature T_o = 5 to 10keV, two different temperature profiles; toroidal mode number n = 10 to 160; aspect ratio 10; major radius R_o = 10 to 20m; central magnetic field B_o = 1 to 2T. In all cases the wave freqeuncy was tuned such that the cyclotron resonance of the minority

passes through the magnetic axis. In Fig.4a the half width s_o was obtained in two independent ways from the comparison between the results of the LION code and the ansatz Eq.(5): firstly from the radius $s = s_{½}$ inside which half the power is absorbed and secondly from the derivative of the Poynting flux at $s = s_{½}$. The error bars in Fig.4a link together both evaluations of s_o. Thus it provides an estimate of how well Eq.(5) can approximate the power deposition profile. In spite of the numerous different cases studied the rather narrow grouping of the points evicences that s_o essentially depends on d for a given antenna. The half width s_o, however, depends also on the type of antenna. Throughout this report we have used the same antenna located on the low field side having a constant unidirectional current. The angular extension of the antenna is from 40° below the midplane to 40° above the midplane measured from magnetic axis. The antenna is described in Ref.[4]. Equation (5) satisfies that $d\bar{P}(0)/ds = 0$ which is necessary in order to have a finite power density on the magnetic axis (see Eq.(4) and Fig.1).

For equilibria with non-circular cross-section or small aspect ratio the flux surface averaged Poynting flux can no longer be approximated by Eq.(5) since the reflected wave is not focused on the magnetic axis. To study such cases we focus our study on typical elliptical JET equilibria and cases where the absorption occurs through a single ion cyclotron resonance passing through the magnetic axis. When analysing the magnetic surface averaged Poynting flux we first study two idealised cases; strong damping and weak damping. We shall later show that the case of finite damping can be expressed as a linear superposition of these two idealised cases.

By strong damping scenarios we mean close to 100% damping of the wave during a single pass. Such scenarios are obtained for minority heating of H at its fundamental cyclotron resonance in a high density D-plasma, $n_D = 10^{14}$ cm^{-3}, with a ratio of $n_H/n_D \approx 0.04$ and $T_H = 10$keV. In this case

the global wave calculation with the LION code verifies the ray tracing picture. The wave is focused on the centre of the plasma where it is absorbed. The position of the focal point will depend on the shape of the cross-section and does not necessarily coincide with the magnetic axis. In case the distance between the focal point and the magnetic axis does not exceed one wavelength the power deposition can be approximated by Eq.(5). As in the circular large aspect ratio case, s_o was obtained from calculations with the LION code for a wide variety of parameters: 3 different equilibria (all of JET-type) were chosen, with a central deuterium density $n_{DO} = 4 \cdot 10^{19}$ to $10^{20} m^{-3}$, two different density profiles; minority temperature T_o = 5 to 20keV; toroidal mode number n = 15 to 70; aspect ratio 2.4 and 2.6, ellipticity 1.4 and 1.68, triangularity 0.19 and 0.4; major radius R_o = 1.5 to 6m; central magnetic field B_o = 1 to 2T; 2 different current profiles. The computed values of s_o are reported in Fig.4b. As in the large aspect ratio case we conclude that s_o essentially depends on d, hence Eq.(5) is a sufficiently good ansatz for the power deposition profile. Moreover, the comparison of Figs.4a and 4b shows that the dependence of s_o on d is the same in both cases.

In the case of incomplete damping of the launched wave, the coupling of the wave by the antennae is characterised by cavity resonances. These are recognised by oscillations of the coupling resistance. The presence of cavity resonances leads to spatial oscillations of the power deposition depending on the position of maxima and minima of the wave field along the cyclotron resonance. For heating scenarios in large tokamaks with at least moderate damping, the antennae couple to a large number of eigenmodes. The oscillations of the wave field along the cyclotron resonance, when summing over the toroidal spectrum, then become small. For such situations one does not need to know the exact wave field at each point of the cyclotron

resonance but it is sufficient to know the value averaged over a wavelength to calculate the power deposition.

To study weak damping scenarios we choose minority heating of H in a D-plasma with a low H/D ratio ~ 10^{-3}. Weak damping is possible to obtain with the LION code for this scenario since the code does not calculate absorption at the harmonics of the cyclotron resonances. No absorption occurs then at the second harmonic of the cyclotron resonance of deuterium, which otherwise could have been fairly strong. In the weak damping case the structure of the wave field varies considerably for small changes in equilibrium parameters or toroidal mode number, depending on which eigenmodes the antennae couple to. We have not found any correlation between the toroidal mode number or coupling resistance with the power deposition. We then take the mean value of the flux surface averaged Poynting flux for some randomly chosen toroidal modes within the launched wave spectrum, such that the contribution to the mean value for each separate mode is small. This is justified when the antennae generate a wide toroidal Fourier decomposition and the absorption coefficient is not too small so that the antenna couples simultaneously to several eigenmodes. We define this mean value $\bar{P}_2(s)$ as the expected resulting Poynting flux. The power deposition is related to $d\bar{P}_2/ds$, which depends on the geometry, the average amplitude of electric field component rotating with the ions along the cyclotron resonance and the local absorption.

We now intend to construct an ansatz expression for the power deposition in case of weak damping. The idea is to separate the effects of the absorption strength and profile from those of the geometry and structure of the wave field. The justification to do so comes from the assumption that for weak damping the structure of the wave field will not change much when the absorption strength and profile vary. We expect only the amplitude of

the wave field to change with absorption. We shall check this assumption later. We first define a parameter which we call the local absorbitivity a(s). The local absorbitivity is the single pass absorption across a corresponding resonant layer in a plane slab geometry having the same densities and temperatures as those on the magnetic flux surface s

$$a(s) = \frac{\omega \int \mathrm{Im}(\underline{E}^* \underline{\underline{\epsilon}} \underline{E}) dx}{2\pi P_x} \tag{6}$$

where the equilibrium quantities may only be inhomogeneous in the x-direction. The magnetic field is perpendicular to the x-direction. The integration is performed across the absorption layer and P_x denotes the x-component of the incident Poynting flux and * denotes complex conjugated quantities. By dividing the power deposition with the absorbitivity a(s) we can then separate the dependence of the field and geometry from the absorption. We call this quantity f(s)

$$f(s) = \frac{C_2}{P_2(1)\, a(s)} \frac{d\bar{P}_2}{ds} \tag{7}$$

where C_2 is a normalisation factor such that $\int_0^1 a(s)\, f(s)\, ds = 1$. Since $\bar{P}_2$ is obtained as the mean value of several toroidal modes for which the position of the maxima and minima of the electric field differs, f(s) is then related to the averaged magnitude of electric field rotating with the ions along the cyclotron resonance and to the geometry, and does not depend on the position of the maxima and minima of electric field.

The procedure to obtain the desired ansatz for weak damping scenarios is the following. First, we compute f(s) according to Eq. (7), where $d\bar{P}_2/ds$ is

calculated with the LION code, for various density profiles and geometries. We shall see that f(s) mainly depends on the density profile but not much on the geometrical parameters of the equilibrium. Then our ansatz will be $d\bar{P}_2/ds$ obtained from Eq. (7) with the calibration curves for f(s) computed before.

In Fig. 5 we show f(s) as calculated with the LION code for a few different density profiles having constant n_H/n_D ratios. The shape of f(s) can be understood by analysing the electric field in a quasi- homogeneous cylinder for which we decompose the wave field as $\exp\left[i(\omega t - k_z z - \frac{m}{r}\theta)\right]$. The resulting ordinary differential equation describing the wave equation can then be solved with the WKB-method for small k and m, i.e. $k_z^2, \frac{m^2}{r^2} \ll \left|\frac{\omega^2}{c^2}\varepsilon_{rr}\right|$. The amplitude of the radial electric field component is then given, for $r \neq 0$ and $n_e \neq 0$, by $E_r = E_o/(r^{1/2} n_e^{1/4})$. Near the centre where $r \approx 0$ and near the cut-off at the plasma boundary where $n_e \approx 0$, the WKB method is not valid and the electric field stays finite. We note in Fig. 5 that f(s) goes to zero when s goes to zero. This is merely a consequence of the fact that the power density p (Eq. 4) is finite, hence $d\bar{P}_2/ds$ (Eq. 7) must go to zero when s goes to zero.

By varying a(s) along the cyclotron resonance, e.g. by multiplying the antihermitian part of the dielectric tensor by an arbitrary function g(s), we have verified that f(s) stays roughly constant as we assumed for the construction of our ansatz.

We have also calculated f(s) for equilibria with a circular cross-section with the same aspect ratio and found that the shape of f(s) does not vary significantly. We conclude that f(s) is not too sensitive to the equilibrium parameters except to the density profile.

To determine $\bar{P}_2$ from Eq. (7) when f(s) is known requires only that we

know a(s) up to a proportionality factor. For heating at the cyclotron resonance of a minority species with low concentration a(s) is proportional to the minority density. For heating at the second harmonic cyclotron resonance, $\omega=2\omega_{c\alpha}$, a(s) becomes proportional to $n_\alpha k_\perp^2 T_\alpha$, where α denotes the heated species; $k_\perp$ is the wave number perpendicular to the magnetic field, n_α and T_α are the density and temperature of the heated species.

For the general case of medium strong absorption we make the following ansatz for the flux surface averaged Poynting flux, $\bar{P}(s)$

$$\bar{P}(s) = \bar{P}_o\left(\alpha\, \bar{P}_1(s) + (1 - \alpha)\, \bar{P}_2(s)\right) \tag{8}$$

where $\bar{P}_1(s)$ is given by Eq. (5), $\bar{P}_o$ is the total power $\bar{P}(s=1)$ and $\bar{P}_2(s)$ is given by Eq. (7) where we choose the constant C_2 such that $\int f(s)a(s)ds = 1$. The parameter α has then to be determined.

To determine α we try to decompose the flux surface averaged Poynting flux as calculated with the LION-code according to Eq. (8). Since an arbitrary function cannot be described by the sum of the two prescribed functions $\bar{P}_1$ and $\bar{P}_2$, such a decomposition can in the best case only be approximately correct. For $s \gg s_o$ we have $\bar{P}_1 \approx 1$, we can then define $\alpha(s)$ as

$$\alpha(s) = \frac{\bar{P}(s)/\bar{P}_o - \bar{P}_2(s)}{1 - \bar{P}_2(s)} \tag{9}$$

where $\bar{P}(s)$ and $\bar{P}_o$ are results of the LION code, whereas $\bar{P}_2(s)$ is obtained according to the ansatz formula for weak damping, Eq.(7) with the calibration curves of Fig.5 for f(s).

The function $\alpha(s)$ oscillates because Eq.(8) does not exactly describe

the code calculations. We take α as the mean value of $\alpha(s)$ for $s >> s_o$. From code calculations with LION we have found that α depends on the damping of magnetosonic waves. To quantify this dependence we have to define a damping coefficient. However, to define a damping coefficient in toroidal geometry is not trivial. Instead we calculate the damping coefficient in a plane slab geometry with the parameters related to that of the midplane with the 1-D global wave code ISMENE [7].

The damping coefficient, a_{IS}, is obtained by decomposing the global 1-D solution into an incident wave of amplitude I and a reflected wave of amplitude R. The damping coefficient is then defined as $a_{IS} = 1 - R^2/I^2$. We note here that I and R are the amplitudes that one would obtain after an infinite number of passes if they were calculated using the WKB approximation. The coefficient a_{IS} can be related to the damping coefficient for a single pass, a_s, by calculating the incident and reflected waves for an infinite number of passes. If interference between the waves is neglected, one obtains

$$a_s = 1 - \sqrt{1 - a_{IS}}\,. \tag{10}$$

The power absorbed at its first pass, P_s, can then be related to the incident wave field I for an infinite number of passes

$$P_s = \left(1 - \sqrt{1 - a_{IS}}\right) a_{IS}\, I^2. \tag{11}$$

By computing $\bar{P}(s)$ with the LION code for plasmas having constant density and temperature profiles, so that a(s) is constant along the cyclotron resonance, and varying the minority concentration, we find a relation between α and a_{IS}. The calculated points are indicated by crosses in Fig.6. We note

here that when calculating the damping coefficient a_{IS} with the ISMENE code this coefficient also becomes sensitive to the equilibrium which makes it more difficult to establish the relation between α and a_{IS}. In Fig.6 we have also plotted the fraction of the power absorbed at its first pass (continuous line). We conclude that this curve approximates α rather well. Implying that the power absorbed according to Eq.(5) is the wave power absorbed when the wave first passes the cyclotron resonance. We thus approximate α with

$$\alpha \approx a_{IS} \left(1 - \sqrt{1 - a_{IS}}\right), \tag{12a}$$

or

$$\alpha \approx a_S \left(2a_s - a_S^2\right), \tag{12b}$$

depending on how we calculate the damping coefficient.

Thus, the determination of the flux surface averaged Poynting flux in toroidal geometry, for any scenario where the cyclotron resonance passes through the magnetic axis, has been reduced to the 1-D global computation of the damping coefficient, a_{IS}, and to the calculation of local absorption coefficients a(s). The 1-D global calculation of a_{IS} can be replaced by the evaluation of the single pass damping coefficient a_s by means of Eq.(10). The proposed formula is Eq.(8), with α given by Eq.(12), $\bar{P}_1(s)$ by Eq.(5) and the calibration curve of Fig.4 for s_o, $\bar{P}_2(s)$ by Eq.(7) and the calibration curve of Fig.5 for f(s).

The model has been tested for a large number of heating scenarios with the LION-code and the comparison is good. We note here that in cases of weak absorption one does not expect the formula to agree too well with the calculated magnetic surface averaged Poynting flux, due to the earlier

mentioned oscillations of the power deposition due to the global mode structure. In the case of weak absorption one should compare the formula with the magnetic surface averaged Poynting flux averaged over different toroidal modes.

Thus when comparing the code result with the model we calculate the flux surfaced averaged Poynting flux given by the formula for a specific toroidal mode number and compute with the LION code the Poynting flux for a few similar toroidal mode numbers to show the scattering in the Poynting flux due to variation of the field structure. To compare the formula and calculations with the LION-code we have chosen three heating scenarios which have rather different power depositions but the same density profile $n_j = n_{oj}(1 - 0.9s^2)^{0.55}$ where j denotes electrons and ion species. This density profile is typical for JET discharges. The first case is fundamental cyclotron resonance heating of H in ^{3}He plasma with the following parameters, $n_H(o) = 2\times10^{11}cm^{-3}$, $n_{He}(o) = 10^{13}cm^{-3}$, $n_c(o) = 1.07\times10^{12}cm^{-3}$, f = 33MHz and T_H = 10keV. This heating scenario has a rather weak damping a_{IS} = 0.35 for $|n| \approx 30$ where the damping coefficient a_{IS} is calculated with the ISMENE code. The comparison with the LION code calculations is shown in Fig.7a. The results of the model are given by the crosses and the results of the code by the lines, for a few toroidal mode numbers.

In the second case we chose a heating scenario with strong absorption a_{IS} = 0.9 which is obtained for fundamental cyclotron heating of H in a D-plasma with the following parameters: $n_H(o) = 3.7\times10^{11}cm^{-3}$, $n_D(o) = 1.84\times10^{13}cm^{-3}$, $n_c(o) = 1.1\times10^{12}cm^{-3}$, f = 33MHz, T_H = 10keV and $|n| \approx 15$ (see Fig.7b).

As the third example we chose an artificial heating scenario having weak absorption but where we multiply the antihermitian part of the dielectric tensor with a function g(s). We chose $g(s) = (1 + 10s^2)$ to change the form of a(s) and make the power deposition less peaked. The variation of the

absorption along the cyclotron resonance is then given by $a(s) \propto n_H(s)\cdot(1 + 10s^2)$. The following parameters have been chosen for this scenario: fundamental heating of H in a D-plasma $n_H(0) = 0.75\cdot10^{11}cm^{-3}$, $n_D(0) = 0.3\cdot10^{14}cm^3$, f = 33MHz and T_H = 10keV. The damping a_{IS} = 0.35 for $|n|$ = 20. The comparison is shown in Fig.7c.

We have studied how the power deposition in the central and outer parts of the plasma varies with the absorption coefficient. Fig.8 shows the fraction of power absorbed inside the surface s = 0.3 and outside the surfaces s = 0.8 and s = 0.9 as calculated with the formula as a function of the damping coefficient $a_{IS}$for a density distribution $n_i = n_o(1 - 0.9s^2)^{0.55}$. For these calculations we assume the absorption coefficient a(s) to be proportional to the electron density. To include the effect of a wide toroidal spectrum as obtained for typical JET antennae we take for the magnetic surface averaged Poynting flux the mean value of three toroidal mode numbers n = 10, 20 and 30. As can be seen from Fig.8, the power deposition in the centre varies slowly with respect to the absorption coefficient whereas the absorption in the outer parts of the plasma decreases rapidly as the damping coefficient increases. The absorption in the outer parts of the plasma can then lead to the creation of high energy particles which interact with the wall or limiters.

3. Power deposition for off-axis heating

To calculate the power deposition when the cyclotron resonance does not pass through the magnetic axis the method described in the previous section can still be used. However, new expressions for the magnetic surface averaged Poynting flux $\bar{P}_1$ and $\bar{P}_2$ have to be obtained which depend on the position of the cyclotron resonance. Here we limit the calculations to particular JET equilibria having ellipticities of 1.4 and 1.68,

triangularities of 0.19 and 0.3, aspect ratios of 2.6 and 2.4 and a density profile of the form $n = n_o(1 - 0.9s^2)^{0.55}$. The power deposition is expected to be a sensitive function of the position of the cyclotron resonance. To label the position of the cyclotron resonance we define s_ω as the magnetic surface which is tangent to the cyclotron resonance.

For the strong damping case we approximate the flux surface averaged Poynting flux, $\bar{P}_1(s)$, by the following ansatz

$$\bar{P}_1(s) = \begin{cases} \bar{P}_1(1) \left\{ \dfrac{1 - \exp\left[-\left(\dfrac{s-s_1}{s_o}\right)^2 \ell n2\right]}{1 - \exp\left[-\left(\dfrac{1-s_1}{s_o}\right)^2 \ell n2\right]} \right\} & s \geq s_1 \\ 0 & s < s_1 \end{cases} \tag{13}$$

The parameters s_o and s_1 are determined by comparing $\bar{P}_1(s)$ and $d\bar{P}_1/ds$ with those calculated with the LION-code at the point where $\bar{P}_1(s) = 0.5 \times \bar{P}_1(1)$. For cases where the cyclotron resonance passes on the low field side (LFS) of the magentic axis, we show in Fig.9 the parameter s_1 versus s_ω for various toroidal mode numbers, temperatures and equilibria. The narrow crowding of the points shows that s_1 is rather independent of the Doppler broadening $d = n\sqrt{\langle v_\parallel^2 \rangle}/\omega r_o$ but essentially depends on s_ω. Fig.9 shows that the power deposition in the centre drops very rapidly as the position of the cyclotron layer is moved out. The parameter s_o, when plotted against d, shows the same dependence as in the on-axis case (Fig.4). We conclude that in this case also s_o essentially depends on d. If we now move the position of the cyclotron layer on the high field side (HFS) of the magnetic axis we find a more complicated dependence for s_o and s_1. What happens is that the

focal point of the magnetosonic wave almost coincides with the geometrical centre of the discharge, which is on the HFS of the magnetic axis for all equilibria that we considered. When s_ω comes close to the focal point s_o decreases and s_1 remains well below the LFS case shown in Fig.9. When s_ω is moved further on the HFS both s_o and s_1 increase rapidly. The fact that the relative positions of the magnetic axis and the focal point depend on the equilibrium keeps us from defining a simplified formula which would be general. Nevertheless we can evidence the qualitative dependence of the power deposition profile: it remains highly centrally peaked when the position of the cyclotron layer is inbetween the geometrical centre and the magnetic axis. For more off-axis cases the power deposition in the centre drops very rapidly as s_ω increases. We were able to quantify this effect only when s_ω is on the LFS of the magnetic axis.

The ansatz for the flux surface averaged Poynting flux for weak damping, $\bar{P}_2$, is calculated in a similar way to on-axis heating (see Eq.7). One might expect the function f(s) to have a rather complicated form which depends on the position of s_ω as well as d. Thus when defining the mean value of $\bar{P}_2$ we take the mean value of randomly chosen densities of the majority species rather than randomly chosen toroidal mode numbers. However, we have found that f(s) is not too sensitive to d. Having realised that we then calculate f(s) by choosing the toroidal mode number n randomly as for the on-axis case. In Fig.10 we show f(s) for different s_ω. A useful approximation of f(s) is

$$f(s) = \begin{cases} \dfrac{s}{s_\omega + \delta} \exp\left\{-\left(\dfrac{\delta + s_\omega - s}{s_f}\right) \ell n 2\right\} & s \leq s_\omega + \delta \\ 1 & s > s_\omega + \delta \end{cases} \qquad (14)$$

Typical values for δ and s_f are $\delta = 0.05$ and $s_f = 0.08$.

We note here that $f(s) \to 0$ when $s_f \to 0$. This should not be interpreted as the wave field vanishes at the magnetic axis for off-axis heating but is merely an effect of our definition of a(s) by Eq.(6). This definition does not depend on the position of the magnetic axis with respect to the cyclotron resonance.

For off-axis heating our formula for the flux surface averaged Poynting flux consists of Eq.(8) where α is given by Eq.(11), $\bar{P}_1$ by Eq.(13), $\bar{P}_2$ by Eq.(7) with f calculated from Eq.(14). s_1 and s_o are obtained from Figs.9 and 10, respectively. To illustrate the comparison between the $\bar{P}(s)$ as calculated with the LION-code and with the formula, we chose a strong damping scenario of minority heating of H in a D-plasma having $a_{IS} = 0.9$ which is obtained for the following parameters: $n_H(o) = 4.2\times10^{11}cm^{-3}$, $n_D(o) = 2.1\times10^{13}cm^{-3}$, $n_c(o) = 1.3\times10^{12}cm^{-3}$, $B_o = 2.17T$, $f = 28.5MHz$, $T_H = 10keV$, and $|n| \approx 15$. The comparison between the formula and code calculations is shown in Fig.11.

4. Discussion

The power deposition for ion cyclotron heating in a tokamak plasma has been analysed. In the case of weak dispersion the power deposition in large aspect ratio equilibria with circular cross-sections is qualitatively different compared to that of other equilibria or for strong dispersion of the wave for a large aspect ratio. This can be understood by the lack of focusing of the reflected wave. In the former case the power deposition depends essentially on the Doppler broadening of the cyclotron resonance whereas in the other cases it also depends on the damping coefficient. Heuristic formulae for the power deposition in equilibria with large aspect ratio and circular cross-section and in elongated equilibria of JET-type

based on calibration curves and functions calculated with the LION-code have been given. The problem of calculating the power deposition is then reduced to calculating the launched toroidal wave spectrum, the damping and the local absorption coefficient.

To calculate the power deposition for a realistic antenna, the antenna current must be decomposed in a Fourier series in the toroidal direction. The power deposition can then be calculated by superimposing the power deposition profiles for the various toroidal mode numbers after they have been weighted by the square of the Fourier amplitudes.

As expected, the power deposition is most sensitive to the position of the cyclotron resonance (see Eq.(13) and Fig.9). The power deposition near the magnetic axis for on-axis heating scenarios does not depend too much on the single pass damping for minority heating scenarios where the absorption is proportional to the minority density. However, the absorption at the plasma boundary increases significantly as the damping decreases.

The formulae derived for the magnetic surface averaged Poynting flux should be regarded to approximate the expected value of the magnetic surface averaged Poynting flux. For weak damping the power deposition, as calculated with the LION code, fluctuates depending on which eigenmodes the antenna couples to. The mean value of the magnetic surface averaged Poynting flux, calculated for slightly different equilibria or toroidal mode numbers, agrees better with the formulae. For large tokamaks and for heating scenarios with at least a moderate damping, the antenna will couple to a large number of eigenmodes and the resulting power deposition will not be too sensitive to the equilibrium parameters. For small tokamaks and for heating scenarios with relatively weak damping the antenna couples only to a few eigenmodes and the power deposition may vary as the equilibrium parameters change; it is in particular sensitive to variation of the average density.

A technichal disadvantage of global wave codes being based on a flux coordinate system is that close to the plasma boundary the mesh points become less dense, where the absorption layer is thinnest due to the lower temperature. This problem can partly be handled by making the mesh more dense at the cyclotron layer. To have good resolution the temperature must be chosen sufficiently high to provide resolution of the absorption layer through the whole plasma. Since the formula only depends on the local absorption, the simplified formula can be extrapolated into regimes where the code resolution becomes too poor, or to heating scenarios which the code cannot handle, such as heating at the second harmonic.

The formula is restricted to the case when the antenna is placed on the low field side and cannot be used for heating scenarios where the magnetosonic wave is directly damped by transit time damping. Deviations from the formula are expected in cases where most of the wave is damped before reaching the cyclotron resonance or in the case of large density gradients such as the ones produced by pellet injections which will focus the wave more sharply on the magnetic axis.

When mode conversion is present, the converted wave could convert a part of the energy away from the resonance and modify the power deposition profile. These effects are not included in our model. The problem of simultaneous mode conversion and cyclotron damping is not a trivial problem and up to now has not been solved in toroidal geometry including the equilibrium poloidal magnetic field.

References

[1] BRAMBILLA, M. RAYC - A Numerical Code for Study of Ion Cyclotron Heating of Large Tokamak Plasma. Max-Planck Institut für Plasmaphysik, Garching, IPP 4/216 (1984).

[2] KOCH, R., BHATNAGAR, V.B., MESSIAN, A.M. and van ESTER, D. Computer Physics Communications 40 (1986) 1.

[3] ITOH, K., ITOH, S.-I. and FUKUYAMA, A. Nucl. Fusion 24 (1984) 13.

[4] VILLARD, L., APPERT, K., GRUBER, R. and VACLAVIK, J. Comput. Phys. Reports 4 (1986) 95.

[5] JAEGER, E.F., BATCHELOR, D.B., WEITZNER, H. and WHEALTON, J.H. Computer Physics Communications 40 (1986) 33.

[6] APPERT, K., COLLINS, G.A., HELLSTEN, T., VACLAVIK, J. and VILLARD, L. Plasma Physics and Controlled Fusion 98 (1986) 133.

[7] APPERT, K., HELLSTEN, T., VACLAVIK, J. and VILLARD, L. Computer Physics Communications 40 (1986) 73.

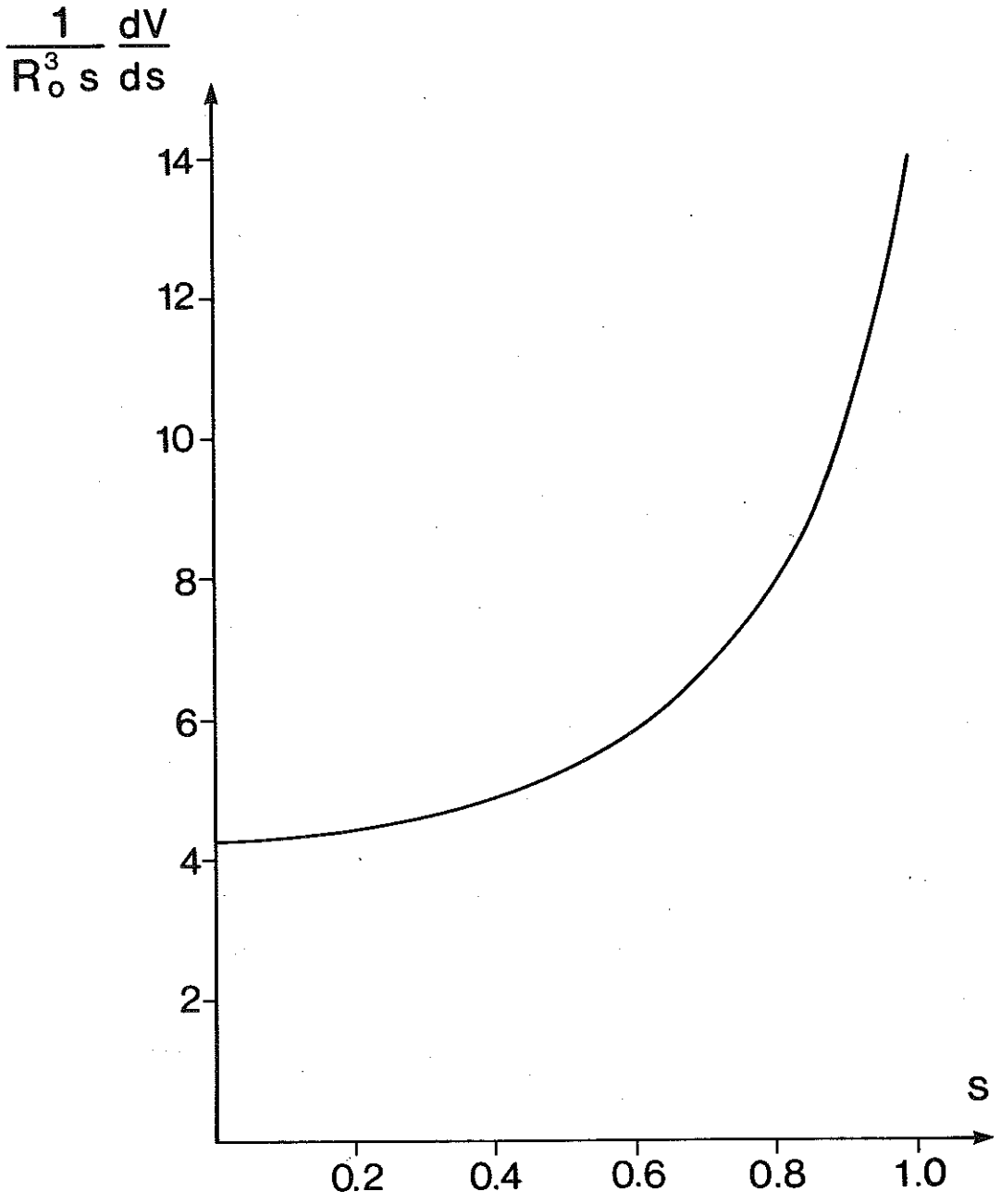

Fig.1 The function $(dV/ds)/R_o^3 s$ versus s for an elliptic JET equilibrium.

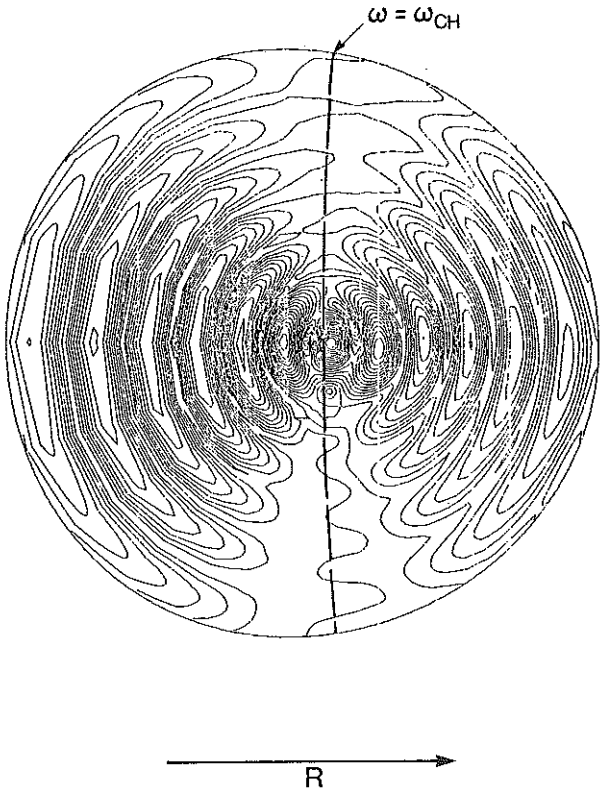

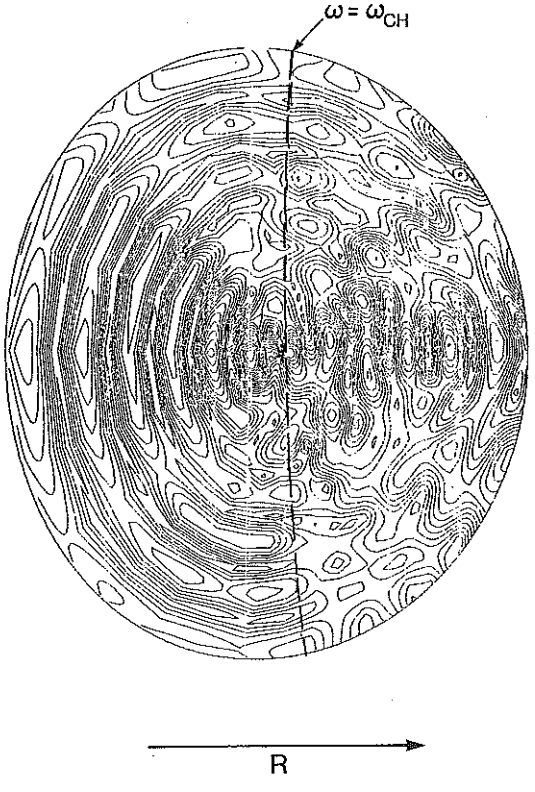

Fig.2 Level surfaces of the electric field $|E_+|$ for minority heating of hydrogen at fundamental cyclotron resonance in a D-plasma.
$n_H = 5\times10^{10}cm^{-3}$, $n_D = 1\times10^{13}cm^{-3}$, n = 30. Aspect ratio of 10.
a) ellipticity = 1.0, b) ellipticity = 1.4.

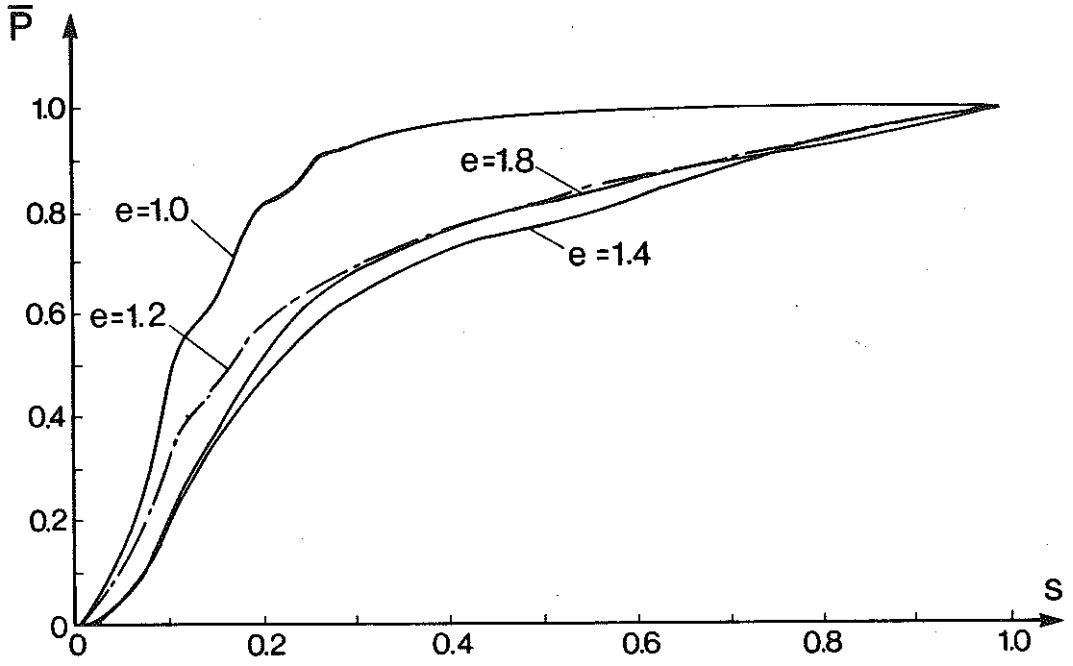

Fig.3 Integrated Poynting flux $\bar{P}$ versus s for different ellilpticities, e, of the cross-section for a plasma of constant density.

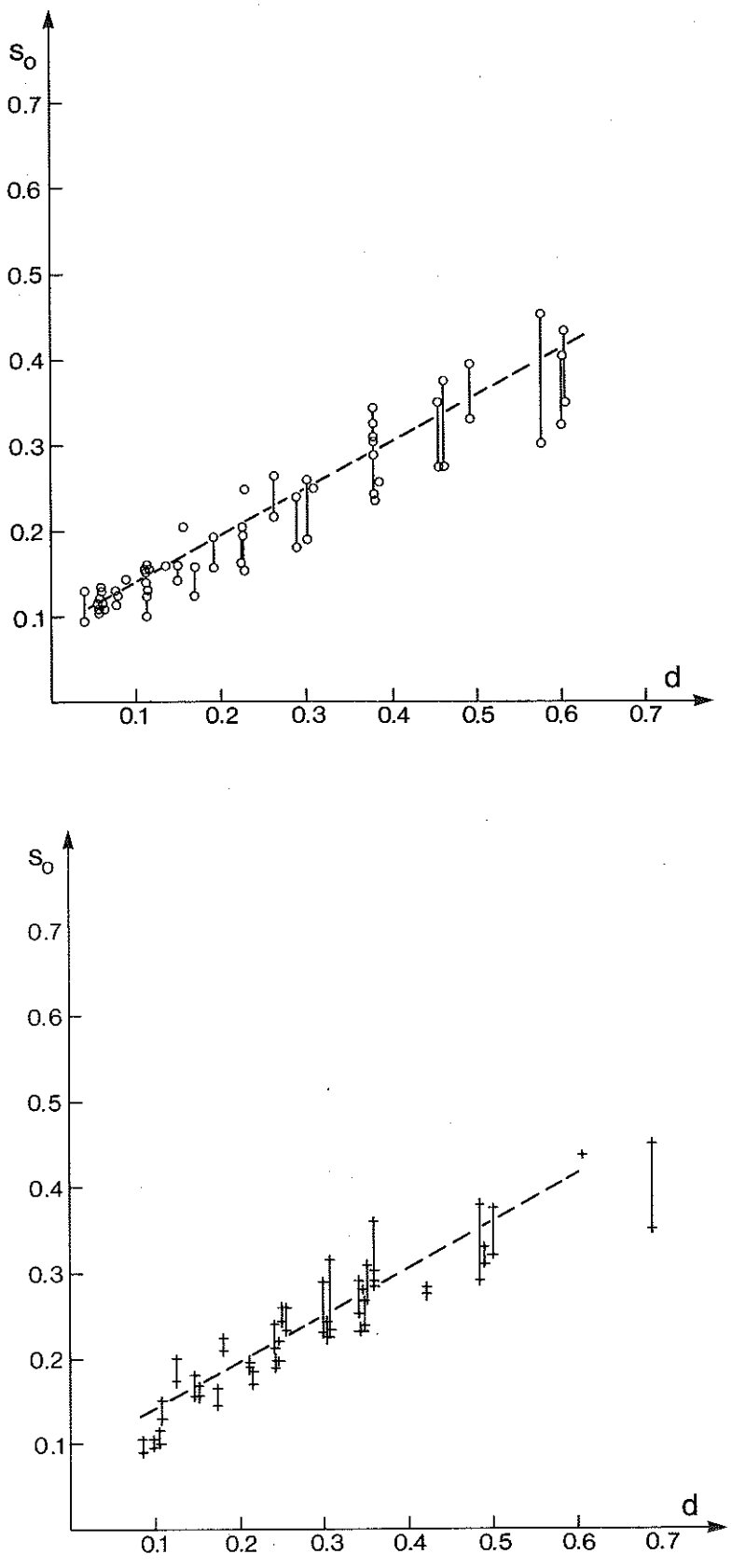

Fig.4 The relation between the half width s_o and d. a) for circular equilibria with large aspect ratio (o). b) for strong absorption scenarios with elliptic cross-section and small aspect ratio (+).

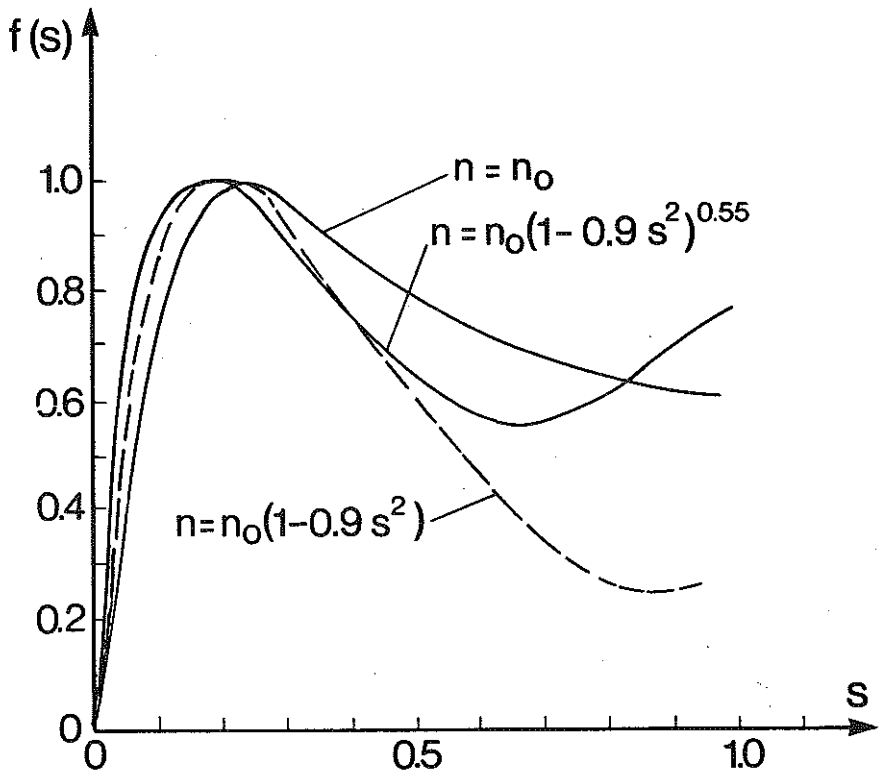

Fig.5 The shape function f(s) determining the power deposition for weak damping cases for various density profiles. f(s) is normalised such that the maximum value equals 1.

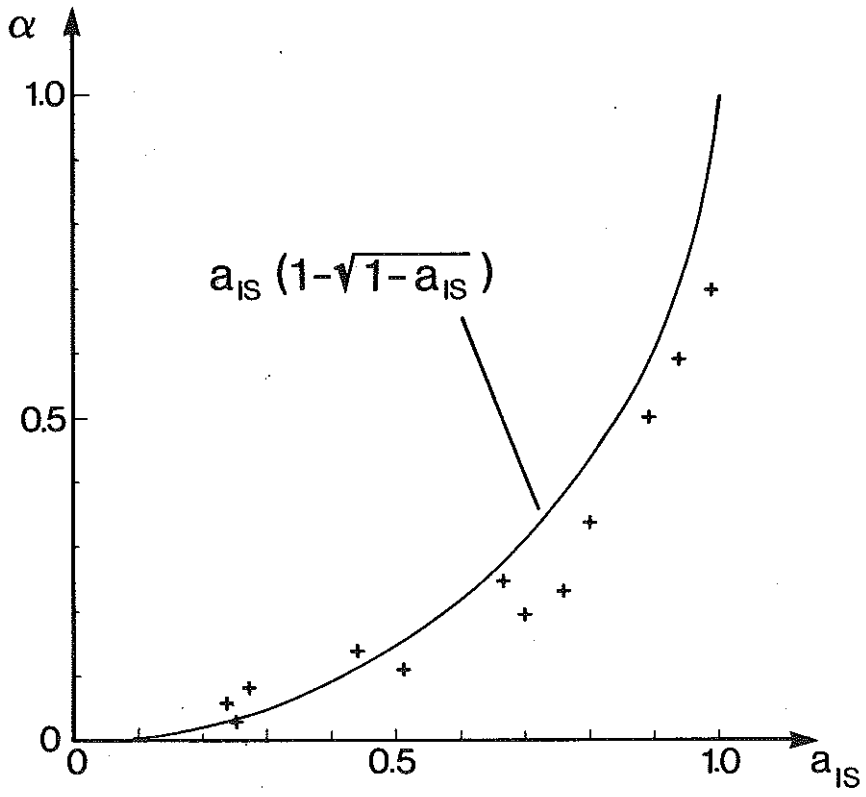

Fig.6 The relation between α and a_{IS}. The crosses are calculated with LION and ISMENE codes. The continuous line is given by Eq. (12a).

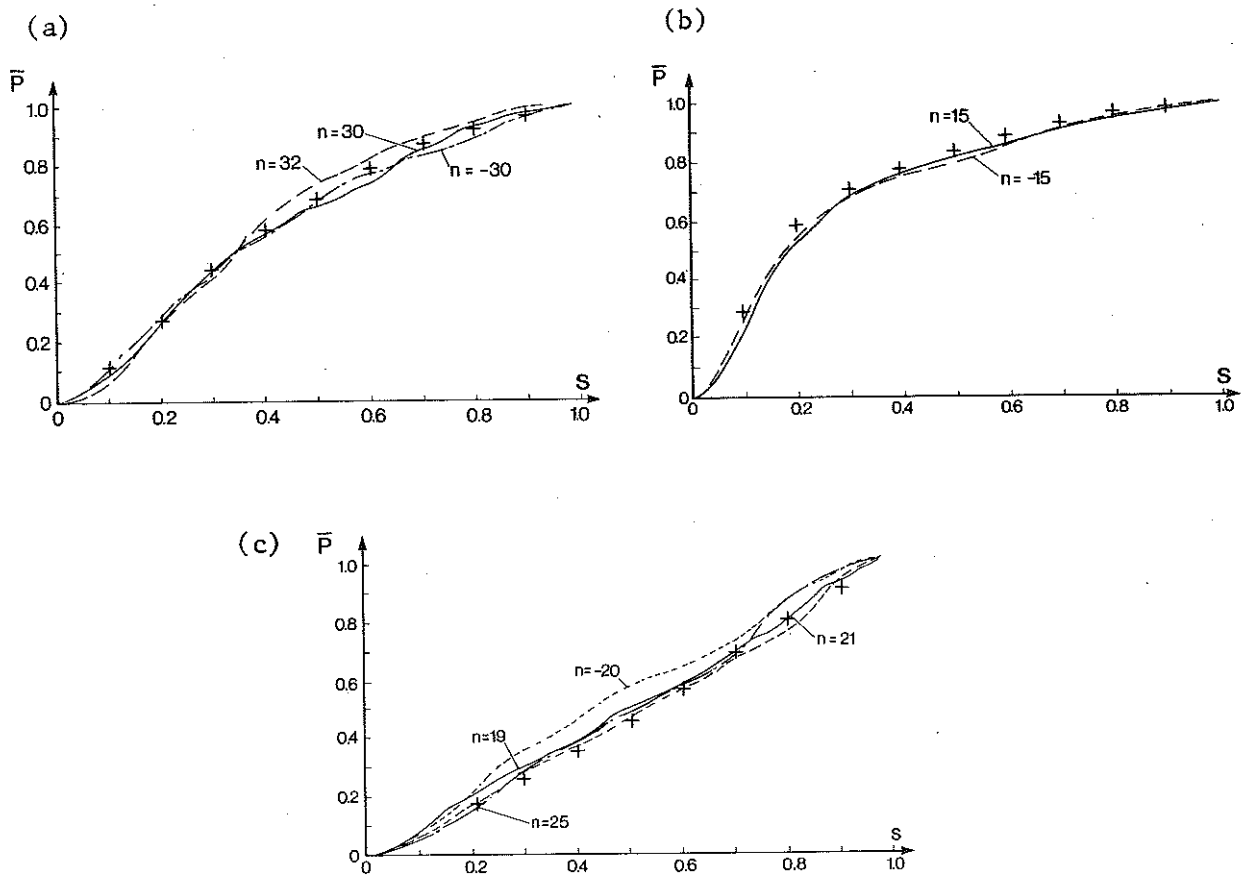

Fig.7 Comparison between numerical calculations of the flux averaged Poynting flux (lines) and the formula (crosses), a) heating of H minority in a ^3H_e-plasma, formula is calculated for n=30, b) heating of H minority in a D-plasma, formula is calculated for n=15, c) an artificial heating scenario, formula is calculated for n=20.

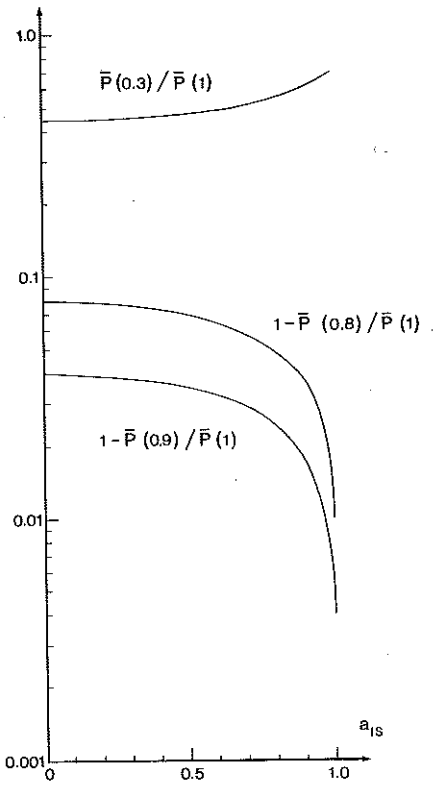

Fig.8 Ratios of absorbed power inside s = 0.3 and outside s = 0.8 and s = 0.9 as a function of a_{IS}, as calculated with the formula.

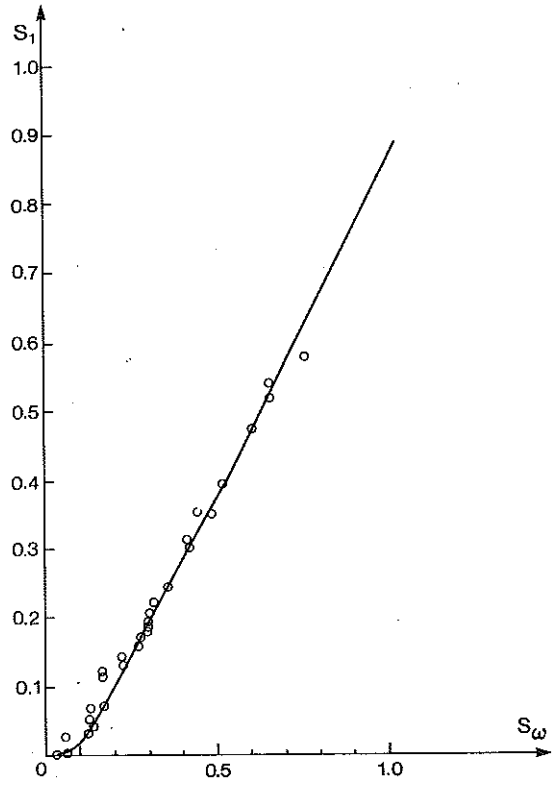

Fig.9 The parameter s_1 versus s_ω for various temperatures and toroidal mode numbers.

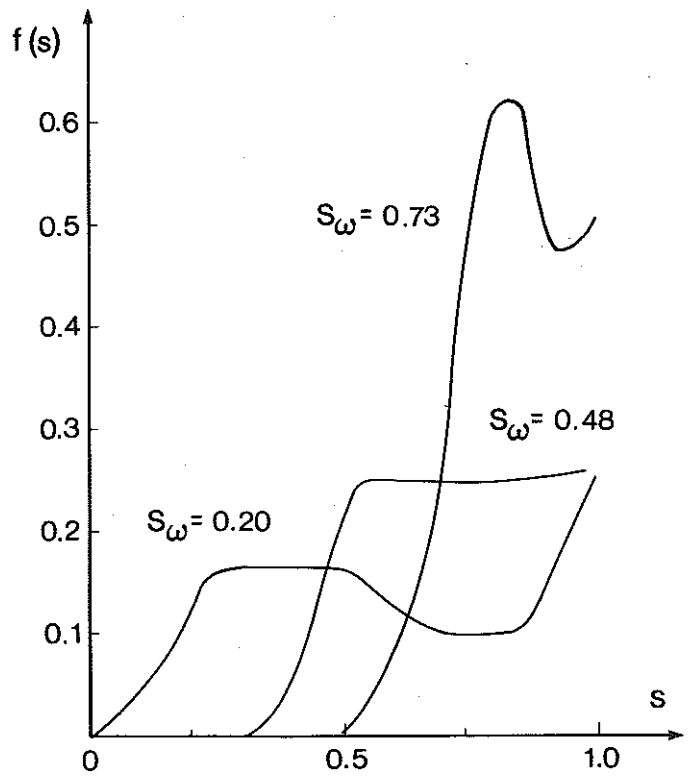

Fig.10 The shape function f(s) determining the power deposition for weak damping for various s_ω.

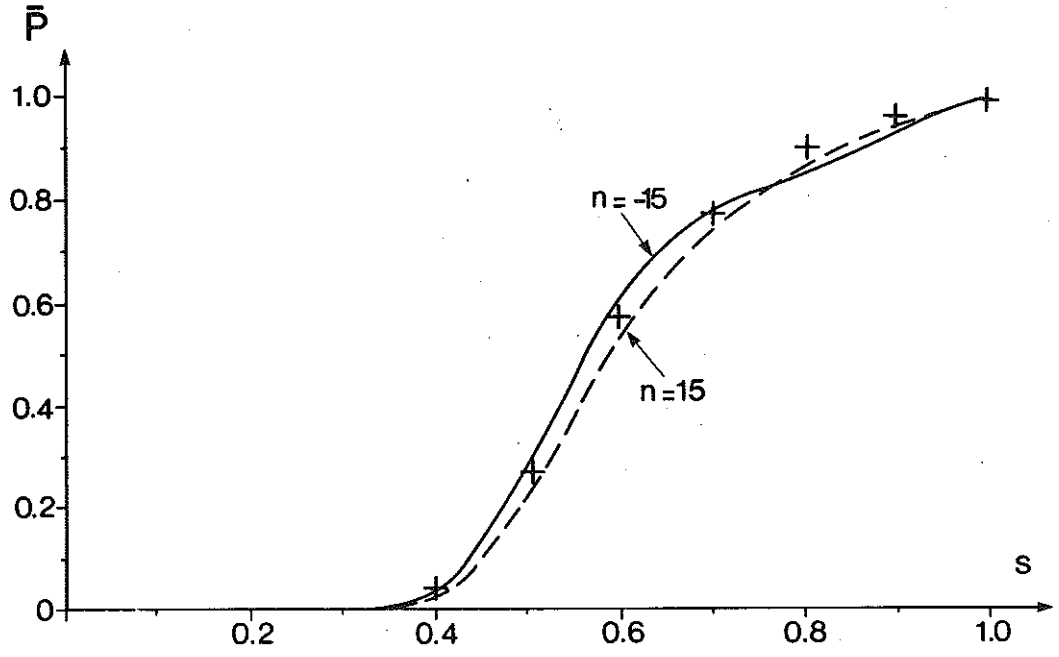

Fig.11 Comparison between numerical calculations of the flux averaged Poynting flux (lines) and formula (crosses) for off axis heating.